Available online at www.sciencedirect.com

ScienceDirect

Procedia CIRP 102 (2021) 7–12

www.elsevier.com/locate/procedia

18th CIRP Conference on Modeling of Machining Operations

Experimental and FEM analysis of dry and cryogenic turning of hardened steel 100Cr6 using CBN Wiper tools

G. Ortiz-de-Zarate[a,*], D. Soriano[a], A. Madariaga[a], A. Garay[a], I. Rodriguez[a], P.J. Arrazola[a]

[a] *Mondragon Unibertsitatea, Faculty of Engineering, Loramendi 4, Arrasate-Mondragón, 20500, Spain*

* Corresponding author. Tel.: +34 943 79 47 00; fax: +34 943 79 15 36. *E-mail address:* gortizdezarate@mondragon.edu

Abstract

Employing cutting fluids in machining processes, especially for difficult-to-cut materials, improves machinability through prolonged tool life, improves surface integrity and chip evacuation. However, like oil and water-based cutting fluids are hazardous to the environment and workers' health, alternative solutions are required. Liquid Nitrogen (LN_2) is a cryogenic fluid that can be an option due to its low boiling point (-197ºC) and the fact it exists in the atmosphere at room conditions. Nevertheless, the feasibility of cryogenic cooling techniques in machining is not fully understood; this is why the Finite Element Method (FEM) could give an insight into the phenomena happening on the tool-chip/workpiece interface. This research aims to compare fundamental and industrial outputs when turning hardened steel 100Cr6 using Cubic Boron Nitride (CBN) inserts with wiper geometry in dry conditions and with cryogenic cooling. For this purpose, turning experimental tests were performed in both cooling conditions varying the cutting speed (150-550 m/min). Machining forces were measured during the tests, and then tool wear, microstructural damage, and residual stresses of the workpiece were characterised. A nose turning (3D) FEM model was also developed to understand the influence of cooling strategy on the outputs measured experimentally.

Keywords: Cryogenic; FEM; Nose turning; 100Cr6; CBN

1. Introduction

Hardened 100Cr6 bearing steel (62 HRC) is a difficult-to-cut alloy due to its high hardness. Machining of hard materials increases cutting forces and accelerates tool wear [1]. As cutting forces increase, so does the energy required to cut the material. Most of the energy in the cutting process is converted into heat, which weakens the tool material's interparticle bonding, further increasing tool wear and worsening the surface integrity of the resultant machined part [1].

To avoid such machinability and also surface integrity problems, extra-hard tool materials, such as Cubic Boron Nitride (CBN) tools, have been used by various researchers [2,3]. Another solution employed when machining difficult-to-cut materials relies on the use of cutting fluids. Oil and water-based cutting fluids show a significant improvement in tool life and surface integrity due to their capability of extracting heat and lubricating the cutting zone [4]. On the downside, these fluids can create several environmental and health problems, such as water pollution and soil contamination at disposal, and generation of fumes, which can be hazardous for workers [5].

Extensive research is being conducted in recent decades to develop new machines and methods to reduce, eliminate, or replace conventional cutting fluids. The use of "sub-zero" cooling by applying liquified gases to the cutting zone has been especially attractive for researchers over other techniques such as Minimum Quantity Lubrication (MQL) [6].

Liquid carbon dioxide (LCO_2) and liquid nitrogen (LN_2) have been researched as sustainable and high-performance cooling alternatives to conventional cutting fluids. The reason for this is the low temperature of these gases and their potentially superior heat extraction capacity compared to traditional cutting fluids. Additionally, these alternative cooling systems also lead to the elimination of hazards at the workplace

2212-8271
10.1016/j.procir.2021.09.002

since the presence of these gases is non-hazardous (they exist in the atmosphere).

Nevertheless, the feasibility of the cryogenic cooling technique is still not fully understood since, as opposed to conventional cooling, cryogenic jet cooling is highly sensitive to the position of the nozzles with respect to the cutting tool and workpiece [7,8]. In some cases, the LN_2 can overcool the workpiece or fail to impinge on the tool-chip interface correctly, leading to adverse results in tool life and surface integrity [9,10].

Finite Element Method (FEM) has been used in many materials and processes to analyse and understand the behaviour of difficult-to-cut materials in machining processes. Nevertheless, there is currently a very small amount of published works that consider the cryogenic coolant effect. Among them, Pusavec et al. [11] numerically predicted the phase and the surface heat transfer coefficient of LN_2 in machining. Once the heat transfer models were verified, they were applied to different surfaces of the cutting tools (rake face and flank face) and in the surface of the workpiece prior to machining. These tests were validated via orthogonal cutting of Inconel 718 under dry and cryogenic conditions. Salame et al. [12] combined FEM and Computational Fluid Dynamics (CFD) modelling for understanding the effect of different nozzle positions on the physical parameters of the fluid coming in contact with the tool-workpiece and the subsequent impact on cutting temperatures and tool wear. They modelled the impingement of the LCO_2 "sub-zero" jet and the stress, temperature distribution, and cutting forces in orthogonal cutting of Ti-6Al-4V. However, the model was not validated experimentally.

The literature review evidences the necessity of gaining knowledge on the phenomena involved in the lubricant-tool/workpiece interface to understand the cooling role in the generation of tool wear and surface integrity.

This research aims to analyse the influence of cooling (dry and LN_2) and cutting speed in fundamental (forces) and industrial outcomes (tool wear, microstructural damage, and residual stresses) while turning hardened steel 100Cr6 with CBN tools. To analyse the physical phenomena that occur in the lubricant-tool/workpiece interface that explains the outputs obtained experimentally, a 3D FEM model for dry and LN_2 cooling conditions was developed.

2. Experimental tests

The experimental tests were carried out in a CNC Fagor 8070 T horizontal lathe, using a PCLN L 2020 K12 tool holder and CNGA120408S01030AWH7015 CBN wiper coated insert (PVD TiN coating thickness of 4±0.5 µm). The workpiece was a bar (Ø89 x 450 mm) of 100Cr6 hardened steel with 62 HRC.

Regarding the cutting conditions, the feed and depth of cut were fixed, while the cutting speed and lubrication were varied. In dry condition, the cutting speed influence was analysed every 50 m/min from 300 to 550 m/min, while with cryogenic cooling, the analysis was extended from 150 until 550 m/min (see Table 1). Two repetitions were done for each cutting condition, machining 30 mm of the bar in the longitudinal direction per test.

Table 1. Experimental cutting conditions.

Cutting condition parameter	Dry	LN_2
Cutting speed, v_c (m/min)	300-550	150-550
Feed, f (mm/rev)	0.2	
Depth of cut, a_p (mm)	0.2	

The LN_2 system supplied cryogenic coolant to the shim of the tool holder (see Fig. 1). This shim had a pilot hole to direct the LN_2 flow to the clearance face of the insert. The aim was to cool the newly machined surface with the LN_2 , while keeping the tool cool. The cooling system had a phase separator which ensured that the nitrogen was supplied in liquid phase to the cutting zone. The setup also incorporated a Kistler 9121 dynamometer to measure the forces in the three directions. The same setup was used for dry tests, removing the LN_2 system.

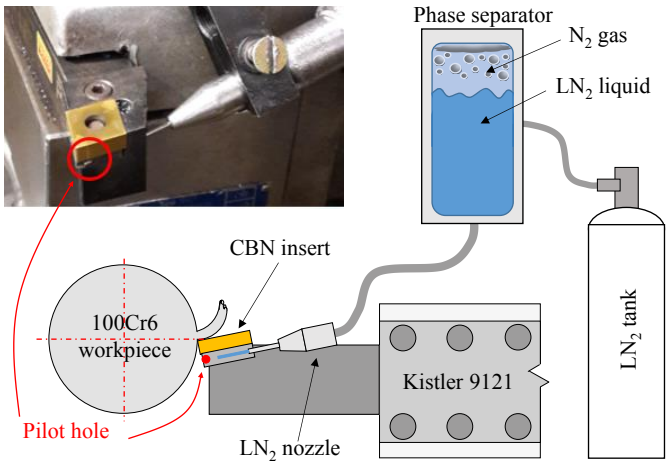

Fig. 1. Experimental setup for LN_2.

After each test, the tool flank wear was measured with an optical amplifier. The microstructural damage of the machined surface was also observed using an optical microscope. For that, cutups in the cutting and feed directions were done, and samples were prepared following conventional metallographic techniques. Additionally, the surface residual stresses were measured by X-ray diffraction in the cutting and feed directions for a single cutting condition (v_c = 300 m/min, f = 0.2 mm/rev, and a_p = 0.2 mm) under dry and LN_2 cooling conditions. A Bruker D8 advance diffractometer was employed for this purpose. The radiation used was CrKα1 with a voltage of 40 kV and a current of 4 mA. The (2 1 1) diffraction plane was chosen for the measurements. A round collimator (2 mm diameter) on the incident beam was used. Measurements were carried out in Ω mode with 14 psi inclinations, ranging from -50º to 50º. Diffraction peaks were fitted with a Pearson VII function that is necessary for eliminating errors from varying blending and defocusing of the Kα doublet diffraction peak [13]. The diffraction elastic constants used in the measurements were: S_1 = -1.271 E^{-6} (MPa^{-1}) and $\frac{1}{2}S_2$ = 5.811 E^{-6} (MPa^{-1}).

3. Finite Element modelling

Deform 3D FEM commercial software was used to develop a 3D nose turning model for dry and cryogenic cooling conditions (see Fig. 2). The software incorporates a lagrangian implicit formulation with remeshing to avoid mesh distortion.

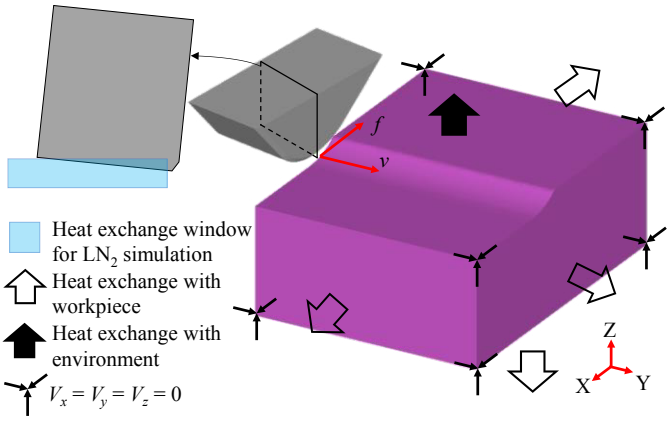

Fig. 2. Boundary conditions of the FEM nose turning model.

The model consists of a rigid tool and an elastoplastic workpiece meshed with 50,000 and 80,000 elements, respectively, with a minimum element size in the workpiece of 10 µm. The remeshing criteria was established to locate the minimum element size in the areas with the higher strain and strain rate, i.e., in the shear regions, including the tool-chip interface, and machined surface.

The tool geometry was characterised using the Alicona IFG4 optical profilometer. First, the 3D geometry of the wiper insert was obtained (Fig. 3a). Then, the rake and relief angles, cutting edge radius, and chamfer geometry were measured (Fig. 3b and Table 2). Using SolidWorks 2020, the tool was modelled (Fig. 3c), and it was imported into the FEM software in STL format. Finally, the tool orientation with respect to the workpiece was corrected in the FEM model to match the tool holder's angles (-6 º axial and radial directions).

Table 2. Wiper insert geometry.

Parameter name	Value
Cutting edge radius, r_β (µm)	33
True negative bevel length, b_γ (µm)	137
Angle of the negative bevel γ_b (º)	30
Clearance angle, α (º)	0
Rake angle, γ (º)	0

Regarding the material properties, the thermo-viscoplastic behaviour of the workpiece was modelled with Johnson Cook's law. The parameters were obtained from Ramesh and Melkote [14]. This material undergoes a softening instead of hardening at high strains (strain softening) [15]. Therefore, a limitation to the yield stress was applied when the plastic strain was greater than one by programing a subroutine in Fortran language. The tool material properties of the CBN were obtained from the library of the software.

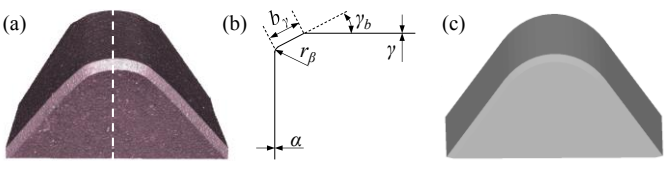

Fig. 3. (a) 3D profile of the tool, (b) tool geometry parameters and (c) SolidWorks model of the tool.

To model the tool-chip contact, the sticking-sliding model was used since it was demonstrated to be the most representative of machining [16]. It was selected the same friction coefficient μ value for both lubrication conditions, since as presented by Hong et al. [17], the application of LN_2 on the clearance face does not produce significant variation of friction with respect to dry machining. They observed that μ varied between 0.38 (LN_2) and 0.48 (dry) at $v_c = 90$ m/min. This could be related to the high pressures in the contact region that does not let the lubrication to reach the cutting zone. At higher cutting speeds, lower friction would be expected due to the increase of the sliding velocity. Therefore, it was selected $\mu = 0.3$ and $m = 1$ for the cutting conditions used in this study.

The difference between dry and LN_2 cooling simulations lies in the boundary conditions applied to the model (see Fig. 2). In both models, the workpiece's movement was restricted in the three directions, and a thermal exchange with the workpiece and with the environment was established. The air convection coefficient used was 20 W/m^{2}K with a room temperature of 20ºC [18]. In the LN_2 cooling simulation, a heat exchange window was included in the flank face of the tool (to reproduce the experimental setup) that moves at the cutting speed (see Fig. 2). In this window, the temperature was -197ºC and the convection coefficient was 5,000 kW/m^{2}K [18].

The simulated cutting conditions were $v_c = 300$ m/min, $f = 0.2$ mm, and $a_p = 0.2$ mm since it is the highest cutting speed in which the tool flank wear is low for both lubrication conditions (see Fig. 4). These conditions were chosen because the purpose of this study is not to analyse the influence of tool wear but the phenomena involved in the lubrication.

4. Results and discussion

4.1. Fundamental variables and tool wear

Fig. 4a shows the influence of cutting speed on maximum experimental cutting (F_c), feed (F_f), and passive (F_p) forces. Fig. 4b presents the tool flank wear for the different cutting conditions tested. In cryogenic cooling, two clear different tool wear regions were observed that match with the force trends. On the one hand, below 300 m/min, homogenous tool wear was reported, and consequently, the cutting speed produces no significant variation in forces, as also observed by [19]. On the other hand, above 300 m/min, a drastic increase of tool wear was observed for the LN_2 cooling conditions that produced the sudden increase of the forces. This could be related to the potential embrittlement of the CBN tool produced by the thermal shock of the cryogenic cooling at high cutting speeds that promotes tool wear (see Fig. 4b,c). This was also observed in the literature on carbide tools [20].

In dry turning, the increase of the cutting speed reduces forces due to the rise of the thermal softening and the decrease of chip thickness, as expected from the literature [21,22]. The tool wear appears not to be significantly affected by the cutting speed (see Fig. 4b,c).

As abovementioned, the comparison between experimental and FEM model results was made for $v_c = 300$ m/min to avoid the drastic tool wear region. The forces of the FEM model were obtained in the thermal steady-state condition, with a machined

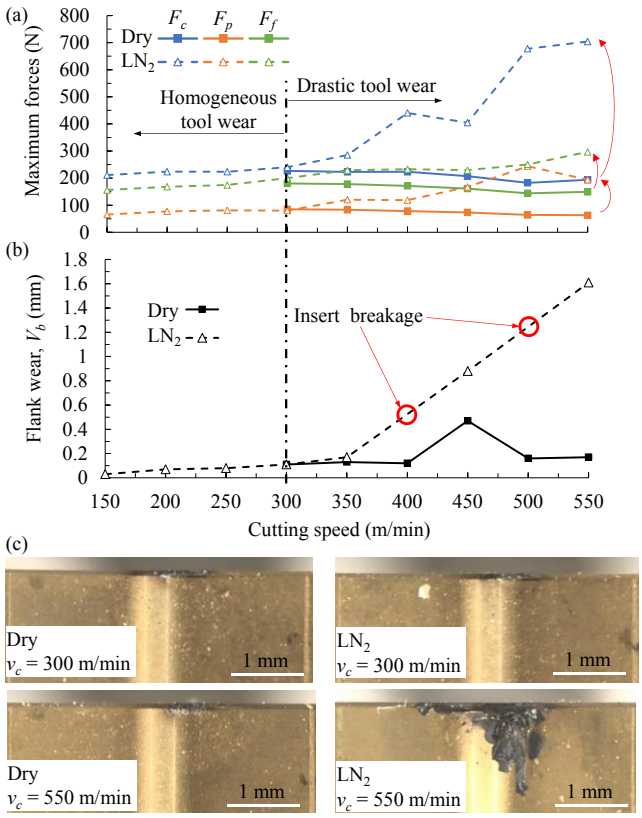

Fig. 4. Influence of cutting speed in (a) maximum forces (uncertainty of 10%) and (b) tool flank wear. (c) Tool flank wear for v_c = 300 m/min and 550 m/min in dry and LN_2.

distance of 2 mm. The FEM model shows the same trends as the experimental results since both reported slightly higher forces for the cryogenic cooling conditions than for dry machining (see Fig. 5). As for the quantitative values, the model predicts lower values than the experimental ones. This might occur because of three main reasons:

- The analysed forces are the maximum, which means that they were obtained at the end of the test, where the tool wear was higher. Although the tool wear for 300 m/min was low (0.13-0.17 mm), it might have influenced the forces.
- It is difficult to ensure that the heat exchange window represents precisely the behaviour of the LN_2 when it impacts the workpiece. In the experimental tests, there may be splashes that could vary the cooling of the tool/workpiece that are not modelled in the FEM approach. The numerical model assumes a very localised and homogeneous impingement of the LN_2 jet (see the cooled region in temperature results of Fig. 6).
- The flow stress and friction parameters were not experimentally characterised. This means that the material parameters might not represent correctly the thermomechanical behaviour of the workpiece material used in the experimental tests.

The FEM model was also consistent in the influence of the cooling in the temperatures. The most significant difference was observed in the temperature gradient along the machined surface (see Fig. 6a,b). Dry condition shows a slow and progressive cooling of the machined surface, while cryogenic results in fast cooling with a high temperature gradient between the tertiary shear zone and the machined surface.

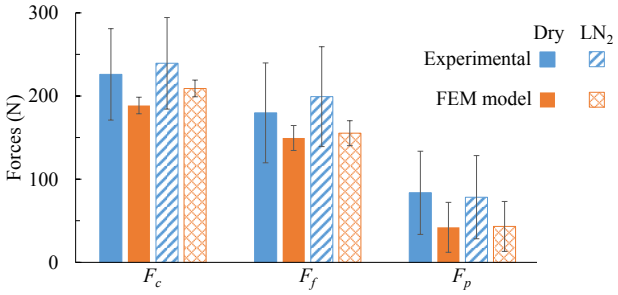

Fig. 5. Experimental and FEM model results of forces (v_c = 300 m/min, f = 0.2 mm, a_p = 0.2 mm).

In the primary and secondary shear zones, the temperature differences were significantly low. As expected, dry condition shows higher temperatures, which is consistent with the force results. However, the differences are not as significant as might be expected. This could be due to the fact that the LN_2 only cools the tool on the flank face, so it reaches the contact area by conduction, reducing its efficiency in cooling the contact area (see Fig. 6c,d). That produces that the tool's maximum temperature is similar in both conditions. The main difference is the higher thermal gradient in cryogenic conditions. This might produce that at higher cutting speeds, where higher contact temperatures are expected, the thermal shock becomes so significant that it could promote drastic tool wear as observed experimentally.

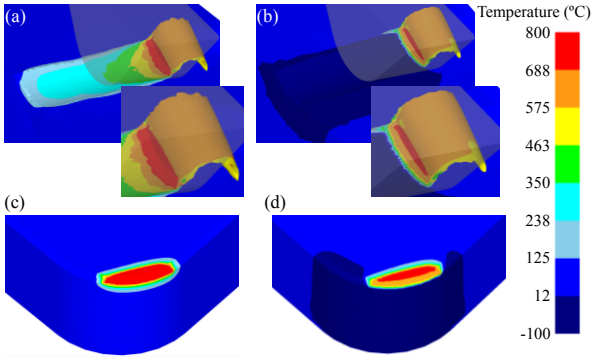

Fig. 6. Workpiece (a,b) and tool (c,d) temperatures in dry (a,c) and cryogenic (b,d) conditions (v_c = 300 m/min, f = 0.2 mm, a_p = 0.2 mm).

4.2. Microstructural damage

The microstructural damage was analysed in the experimental tests observing samples prepared from cutups in the cutting and feed directions (see Fig. 7). The main defects were the presence of a thermally affected layer, white layer, and adhered material. All the machined surfaces had a thermally affected layer in the cutting direction, independent of the cutting speed or lubrication conditions (see Fig. 8).

The cutups in feed direction show step-tool with adhered material only in the surfaces machined with LN_2 at cutting speeds above 400 m/min (see Fig. 7e-h). The frequency of the step-tool matches the feed rate. This could be explained by the drastic tool wear observed at the highest cutting speeds. Moreover, the increase in cutting speed seems to reduce the height of the adhered material, from 16.9 µm for v_c = 400 m/min to 2.6 µm for v_c = 550 m/min.

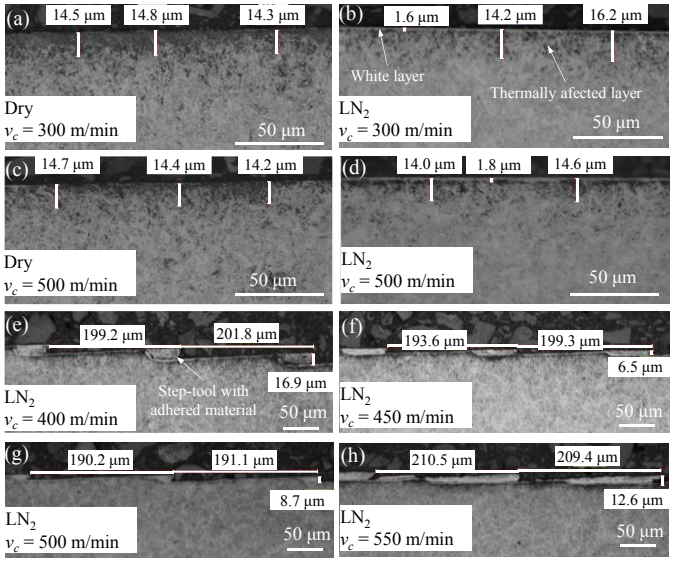

Fig. 7. Cutups in (a-d) cutting and (e-h) feed direction.

Moreover, when machining under cryogenic cooling white layer was observed in most of the cutting speeds, while in dry, it was only found at 400 m/min (see Fig. 8). Generally, the white layer appears in severe cutting conditions (high cutting speed and increased flank wear) when there are high temperatures in the tertiary shear zone. Nevertheless, in LN_2 cooling conditions it can be observed for all cutting speeds (except for 350 and 550 m/min) and even for low tool wear conditions. Kaynak et al. [23] and Pu et al. [24] also observed more significant microstructural damage for LN_2 than for dry for different materials. Furthermore, a similar white layer was obtained for all the cutting conditions tested in LN_2 cooling in this work. Hence, tool wear and cutting speed seem not to significantly affect the white layer depth (see Fig. 8).

To find an explanation for this phenomenon, the strains and temperatures in the machined surface using the FEM model were analysed. The tertiary shear zone temperatures appear to be similar for both cooling conditions (see Fig. 9a,b). Although with LN_2 the cooling effect is drastically higher, it seems that the fluid did not reach the tertiary shear zone due to the high contact pressures of the region. Thus, a similar thermally affected layer would be expected in the machined surface as observed experimentally. Nevertheless, the white layer could not be explained from the surface temperature point of view, and neither from the surface strain, since similar values are reported in the FEM model (see Fig. 9). The only difference

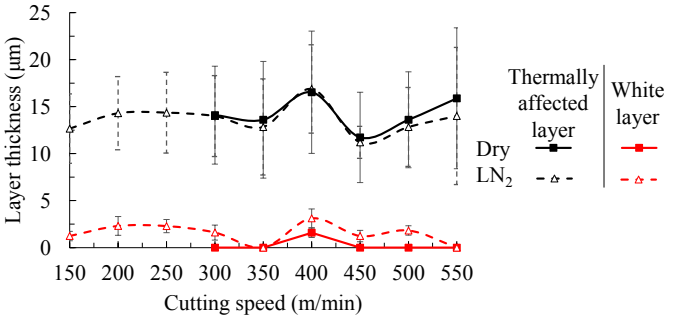

Fig. 8. Influence of cutting speed and lubrication in microstructural damage.

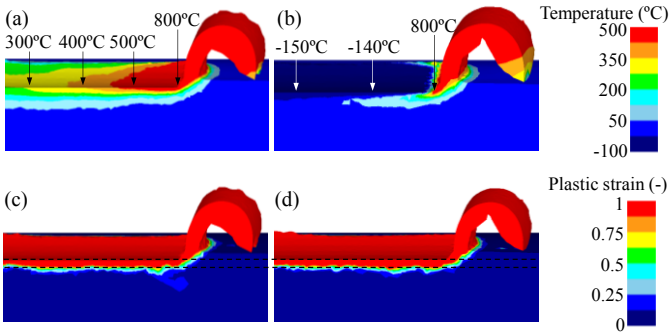

Fig. 9. Temperature (a,b) and plastic strain (c,d) obtained in the machined surface in dry (a,c) and cryogenic (b,d) conditions (v_c = 300 m/min, f = 0.2 mm, a_p = 0.2 mm).

between lubrication conditions is the higher thermal gradient along the machined surface in LN_2 condition that may promote the white layer generation, but more research is needed to confirm this claim.

4.3. Residual stresses

Fig. 10 shows the average values of the residual stresses measured at the surface of the specimens turned using different cooling strategies. Surface residual stresses were tensile in both the cutting (431 ± 130 MPa for dry and 529 ± 84 MPa for LN_2) and feed direction (123 ± 38 MPa for dry and 90 ± 84 MPa for LN_2). It is well known in the field that machining-induced residual stresses have two primary sources: i) thermal loads induce tensile stresses near the surface, and ii) machining forces produce more compressive residual stresses. Therefore, the thermal loads generated during the cutting processes had a greater impact on the surface residual stresses than the machining forces for the tested conditions and material. It should be noted that tensile residual stresses were more tensile in the cutting direction than in the feed direction, which is also in agreement with the literature results.

No significant variations were observed between the cooling strategies since differences are within deviation bars. This finding is in agreement with force measurements and predictions, where no significant differences were detected. Furthermore, simulations also predicted similar contact temperatures in the tertiary shear zone. The slightly higher tensile residual stresses generated by LN_2 in the cutting direction could be attributed to the more rapid cooling as observed in the FEM results. However, this observation needs further analysis, since it is not clear that the fluid reached the tertiary shear zone, as explained in Section 4.2.

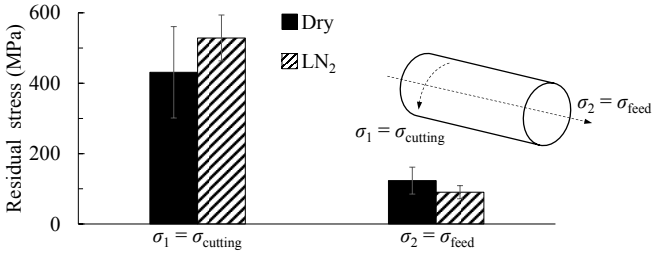

Fig. 10. Surface residual stresses in dry and cryogenic condition (v_c = 300 m/min, f = 0.2 mm/rev, a_p = 0.2 mm).

5. Summary and conclusions

This research work analysed the influence of the cutting speed (150-550 m/min) on fundamental and surface integrity outputs when turning hardened 100Cr6 in dry and cryogenic cooling. A nose turning FEM model to understand the cooling role in the chip formation process and in the generation of surface integrity and tool wear was also developed. The main conclusions of the research are:

- Cryogenic cooling has two different wear regions depending on the cutting speed. Below 300 m/min cutting speed, homogeneous wear is reported, and slightly higher forces than dry condition are obtained. Above 300 m/min, the drastic tool wear increase produces the sudden increase of forces for LN_2 cooling condition. The FEM model shows similar trends when analysing the lubrication's influence at a cutting speed of 300 m/min.
- The microstructural analysis of the machined surface shows a similar thermally affected layer in the cutting direction for both cooling conditions, which might be related to similar temperatures in the tertiary shear zone, as observed in the FEM model. White layer was reported in the cutting direction in most cutting speeds when applying LN_2 cooling, while it was barely observed in dry cutting. Step-tool in feed direction when turning with LN_2 at high cutting speed (in drastic tool wear region) were also observed.
- Higher tensile residual stresses were observed in the surface for cryogenic cooling, which might be produced by the faster cooling of this condition as observed in the FEM results.

Acknowledgements

The authors thank NANOCRIO (KK-2016/00012) and CRYOMACH (INNO-20182049) projects and the grant for Education and Training of Research Staff (PRE_2017_1_0394).

References

[1] Shihab, S. K., Khan, Z. A., Mohammad, A., Siddiquee, A. N. A review of turning of hard steels used in bearing and automotive applications. Production & Manufacturing Research. 2014. 2/1:24-49.
[2] Benga, G. C., Abrao, A. M. Turning of hardened 100Cr6 bearing steel with ceramic and PCBN cutting tools. Journal of materials processing technology. 2003. 143:237-241.
[3] de Siqueira Galoppi, G., Stipkovic Filho, M., Batalha, G. F. Hard turning of tempered DIN 100Cr6 steel with coated and no coated CBN inserts. Journal of materials processing technology. 2006. 179/1-3: 146-153.
[4] Brinksmeier, E., Meyer, D., Huesmann-Cordes, A. G., Herrmann, C. Metalworking fluids—mechanisms and performance. CIRP Annals. 2015. 64/2:605-628.
[5] Pusavec, F., Krajnik, P., Kopac, J. Transitioning to sustainable production–Part I: application on machining technologies. Journal of Cleaner production. 2010. 18/2:174-184.
[6] Kaynak, Y., Lu, T., Jawahir, I. S. Cryogenic machining-induced surface integrity: a review and comparison with dry, MQL, and flood-cooled machining. Machining Science and Technology. 2014. 18/2:149-198.
[7] Lequien, P. Etude fondamentale de l'assistance cryogénique pour application au fraisage du Ti6Al4V. 2017. Doctoral dissertation.
[8] Heep, T., Bickert, C., Abele, E. Application of carbon dioxide snow in machining of CGI using an additively manufactured turning tool. Journal of Manufacturing and Materials Processing. 2019. 3/1:15.
[9] Iturbe, A., Hormaetxe, E., Garay, A., Arrazola, P. J. Surface integrity analysis when machining inconel 718 with conventional and cryogenic cooling. Procedia Cirp. 2016. 45:67-70.
[10] Isakson, S., Sadik, M. I., Malakizadi, A., Krajnik, P. Effect of cryogenic cooling and tool wear on surface integrity of turned Ti-6Al-4V. Procedia CIRP. 2018. 71:254-259.
[11] Pusavec, F., Lu, T., Courbon, C., Rech, J., Aljancic, U., Kopac, J., Jawahir, I. S. Analysis of the influence of nitrogen phase and surface heat transfer coefficient on cryogenic machining performance. Journal of materials processing technology. 2016. 233:19-28.
[12] Salame, C., Bejjani, R., Marimuthu, P. A better understanding of cryogenic machining using CFD and FEM simulation. Procedia CIRP. 2019. 81:1071-1076.
[13] Prevéy, P. S. The use of Pearson VII distribution functions in X-ray diffraction residual stress measurement. Advances in X-Ray analysis. 1986. 29:103-111.
[14] Ramesh, A., Melkote, S. N. Modeling of white layer formation under thermally dominant conditions in orthogonal machining of hardened AISI 52100 steel. International Journal of Machine Tools and Manufacture. 2008. 48/3-4:402-414.
[15] Poulachon, G., Moisan, A., Jawahir, I. S. On modelling the influence of thermo-mechanical behavior in chip formation during hard turning of 100Cr6 bearing steel. CIRP Annals. 2001. 50/1:31-36.
[16] Zorev, N.N. Inter-relationship between shear processes occurring along tool face and shear plane in metal cutting. International research in production engineering. 1963. 49:143-152.
[17] Hong, S. Y., Ding, Y., Jeong, W. C. Friction and cutting forces in cryogenic machining of Ti–6Al–4V. International Journal of Machine Tools and Manufacture. 2001. 41/15:2271-2285.
[18] Pu, Z., Umbrello, D., Dillon Jr, O. W., Lu, T., Puleo, D. A., Jawahir, I. S. Finite element modeling of microstructural changes in dry and cryogenic machining of AZ31B magnesium alloy. Journal of Manufacturing Processes. 2014. 16/2:335-343.
[19] Bogajo, I. R., Tangpronprasert, P., Virulsri, C., Keeratihattayakorn, S., Arrazola, P. J. A novel indirect cryogenic cooling system for improving surface finish and reducing cutting forces when turning ASTM F-1537 cobalt-chromium alloys. The International Journal of Advanced Manufacturing Technology. 2020. 111/7:1971-1989.
[20] Tarragó, J. M., Dorvlo, S., Al-Dawery, I., Llanes, L. M. Strength degradation of cemented carbides due to thermal shock. In Proceedings of the Euro PM2015 Congress & Exhibition. 2015.
[21] Ortiz-de-Zarate, G., Sela, A., Saez-de-Buruaga, M., Cuesta, M., Madariaga, A., Garay, A., Arrazola, P. J. Methodology to establish a hybrid model for prediction of cutting forces and chip thickness in orthogonal cutting condition close to broaching. The International Journal of Advanced Manufacturing Technology. 2019. 101/5-8:1357-1374.
[22] Sela, A., Ortiz-de-Zarate, G., Arrieta, I., Soriano, D., Aristimuño, P., Medina-Clavijo, B., Arrazola, P. J. A mechanistic model to predict cutting force on orthogonal machining of Aluminum 7475-T7351 considering the edge radius. Procedia CIRP. 2019. 82:32-36.
[23] Kaynak, Y., Tobe, H., Noebe, R. D., Karaca, H. E., Jawahir, I. S. The effects of machining on the microstructure and transformation behavior of NiTi Alloy. Scripta Materialia. 2014. 74:60-63.
[24] Pu, Z., Outeiro, J. C., Batista, A. C., Dillon Jr, O. W., Puleo, D. A., Jawahir, I. S. Enhanced surface integrity of AZ31B Mg alloy by cryogenic machining towards improved functional performance of machined components. International journal of machine tools and manufacture. 2012. 56:17-27.